Journal of Applied Polymer Science

Preparation of a Magnetic Chitosan Composite Adsorbent by Ammonia Fumigation

Yong Wang, Xiaopeng Xiong, Weiwei Zou
Department of Materials Science and Engineering, College of Materials, Xiamen University, Xiamen 361005, China
Correspondence to: X. Xiong (E-mail: xpxiong@xmu.edu.cn)

ABSTRACT: A magnetic chitosan (CS) composite material was synthesized successfully by a new procedure, ammonia fumigation, which is suitable for large-scale production. CS dissolved in an aqueous acetic acid solution was mixed with $[Fe(SO_4)_2]^{2-}$ and $[Fe(SO_4)_2]^{-}$ ions to obtain a light yellow precipitate, which was then exposed to ammonia vapor to prepare the composite adsorbent product. The microstructure of the composite was studied by scanning electron microscopy, transmission electron microscopy, X-ray diffraction, and Fourier transform infrared spectroscopy. The results indicate that Fe_3O_4 particles 3–7 nm in size were formed *in situ* and were stabilized in the CS matrix. The composite adsorbent showed superparamagnetic properties with a saturation magnetization of about 11.0 emu/g. Moreover, the composite material displayed good adsorption of methyl orange and copper ions. © 2013 Wiley Periodicals, Inc. J. Appl. Polym. Sci. **2014**, *131*, 40057.

KEYWORDS: chitosan; Fe_3O_4; ammonia fumigation; composite absorbent; absorption

Received 18 July 2013; accepted 11 October 2013
DOI: 10.1002/app.40057

INTRODUCTION

Composite materials are known as the fourth generation of new materials on the basis of their diversity of functions.[1–3] In particular, composite materials have become a well-established platform for the development of environmental protection materials, mechanical materials, membrane materials, biological medicines, protein separation and molecular self-assembly materials[4–12] and have attracted more and more attention.

As a rich source of natural polymer, chitosan (CS) is used as inexpensive sorbent replacement for wastewater treatment applications because of its abundant functional groups, which include amino and hydroxyl groups. These functional groups are also helpful for the stabilization of nanoparticles, so a variety of CS-based nanocomposites have been prepared for various purposes. Magnetic CS composites combine the characteristics of CS and an external magnetic field responsibility; this endows this type of composite material with various applications.[13] If the composite material is nanosized, it has a relatively high surface area and is easily magnetically separated to have great potential as an adsorbent. For example, Chang and Chen[14] prepared CS/Fe_3O_4 composite nanoparticles by the covalent binding of carboxymethylated CS on Fe_3O_4 nanoparticles via carbodiimide activation. The thus prepared nanoparticles were about 13.5 nm with 12-nm Fe_3O_4 and displayed a high adsorption of Cu(II) ion. Wang et al.[15] synthesized magnetic Fe_3O_4–CS nanoparticles with a diameter of 10–20 nm by a microemulsion system. The bovine serum albumin (BSA) adsorption experiment indicated that a maximum adsorption (Q_{max}) of 110 mg/g of BSA could be reached at pH 4. During these preparations, coprecipitation in a homogeneous medium has always been used to obtain the nanocomposites.[13–17] Namely, magnetite precursors and CS have been precipitated simultaneously, and nanoscaled Fe_3O_4 was synthesized *in situ* to obtain the final nanocomposite product. However, these processes were conducted in a water/oil system or with multistep reactions or used special devices, where the emulsifying agents were hard to remove or expensive equipment was required; this limits the practical application of the composite material.

It is known that the amino groups of the CS chain will be protonized and thereafter dissolved in a dilute acid solution so that the cationic CS chains could easily bind negatively charged material to form stable polyelectrolyte compounds. In this study, CS dissolved in an aqueous acetic acid solution was mixed with $[Fe(SO_4)_2]^{2-}$ and $[Fe(SO_4)_2]^{-}$ ions to obtain a light yellow precipitate, and the precipitate was then exposed to ammonia vapor. The precipitation of the iron ions was heterogeneous compared to that in the aforementioned coprecipitation in the homogeneous medium. As a result, the microstructure and the properties of the obtained product were different. Fourier transform infrared (FTIR) spectroscopy, X-ray diffraction (XRD), scanning electron microscopy (SEM), and transmission electron microscopy (TEM) characterizations were carried out for this purpose. Its magnetic properties were also

measured with vibrating sample magnetometry (VSM). The adsorption of the composite material was tested with representatives of copper ions and methyl orange (MO). The preparation of the nanocomposite via the method of ammonia fumigation is thought to be suitable for industrial fabrication.

EXPERIMENTAL

Materials

CS, with a degree of deacetylation of 90%, was purchased from Jinan Haidebei Marine Bioengineering Co., Ltd. (Shandong, China). The viscosity-average molecular mass of the CS was determined in a 0.1 mol/L CH_3COONa/0.2 mol/L CH_3COOH buffer at 30°C to be 1.44×10^5 g/mol according to an intrinsic viscosity of $6.589 \times 10^{-3} \cdot M^{0.88}$.[18] Ammonium ferric sulfate dodecahydrate [$NH_4Fe(SO_4)_2 \cdot 12H_2O$], ammonium ferrous sulfate dodecahydrate [$(NH_4)_2Fe(SO_4)_2 \cdot 12H_2O$], ammonia, acetic acid, ethanol, $CuSO_4$, and MO (reagent grade) were purchased from commercial resources in China. Deionized water was used throughout.

Preparation

A 0.1 wt % CS solution was prepared by the dissolution of CS powder in a 2 wt % acetic acid aqueous solution. Then, a mixed aqueous solution of 0.1 mol/L $NH_4Fe(SO_4)_2$ and 0.05 mol/L $(NH_4)_2Fe(SO_4)_2$ was dropped into the previous CS solution under mechanical stirring at room temperature. A continuous 1 h of stirring was carried out after the total addition of the iron solution (with a volume ratio of 1:5 to the CS solution) to obtain an light yellow precipitate. The precipitate was filtered, washed with water, and then subjected to an ammonia fumigation reaction by positioning it in an ammonia vapor atmosphere for 6 h at room temperature. The obtained dark brown product was washed in turn with deionized water and ethanol three times and then vacuum-dried before characterization.

Characterization

The composite material was sputtered with gold (ca. 2 nm) to observe its microstructures with SEM (JEM-2100, JEOL, Tokyo, Japan).

XRD patterns of pure CS and the composite material were recorded using a PANalytical diffractometer (PANalytical, Netherlands) with CuKα radiation, and continuously scanned from10 to 80° (2θ) at a speed of 0.0167°/s.

FTIR characterization was performed on a Nicolet Avatar 360 instrument (Nicolet, Madison, WI) at 25°C. The samples were first vacuum-dried at 40°C for over 48 h and then ground to mix with KBr to produce disks for the measurements.

TEM was performed with a JEM-2100 electron microscope (JEOL, Tokyo) at 200 kV.

Thermogravimetric analysis (TGA) measurements were performed on a Netzsch 409EP thermal analyzer (Germany) under a nitrogen atmosphere at a heating speed of 10°C/min from 25 to 700°C.

A vibrating sample magnetometer (VSM-5–15, TOEI Industry Co., Ltd., Japan) was used to assess the magnetic properties of the composite material. A certain amount of material was positioned in the magnetometer and was balanced before measurements. We determined the hysteresis of the magnetization by increasing the magnetic field intensity from −20,000 to +20,000 Oe at 27°C, and the magnetic properties were evaluated in terms of their saturation magnetization and coercivity.

Adsorption of Cu^{2+} and MO

A certain amount of the magnetic composite material was immersed into Cu^{2+} or an MO aqueous solution with light stirring for a desired time at room temperature, and then, 5 mL of the supernatant was extracted to determine the concentration of Cu^{2+} at 265 nm[19] or MO at 465 nm[20] with an ultraviolet–visible spectrophotometer (50BIO, Varian, Australia), respectively. The pH of the adsorption solutions was kept around 5.5.

The adsorption efficiency (Q) of the Cu(II) ions and MO were calculated according to the following equation:

$$Q=(C_0-C_e)V/M \quad (1)$$

where C_0 and C_e are the concentrations of the Cu(II) ions and MO before and after adsorption, respectively; V is the volume of the adsorbate solution; and M is the mass of the magnetic composite adsorbent.

RESULTS AND DISCUSSION

Microstructure

The obtained composite material was a dark brown powder, which looked like coffee powder. Figure 1 shows the SEM images of the magnetic CS composite material. As shown in Figure 1(A), the composite was a particulate material ranging from nanometers to micrometers. As shown in Figure 1(B), the composite material displayed a rough surface, which consisted of nanoparticles. This morphology suggested a large specific surface area of the composite material, which was beneficial to its adsorption ability.

Figure 2 shows the XRD patterns of the pure CS and the composite material. The pattern of the pure CS revealed only broad diffraction at a 2θ around 19.8°. The pattern of the composite material exhibited six characteristic peaks at 2θ values of 30.1, 35.6, 43.1, 53.4, 57.0, and 62.6°, which could be indexed to the diffraction planes (220), (311), (400), (422), (511), and (440), respectively, for the crystallized structure of the Fe_3O_4. The results indicate that the composite consisted of CS and Fe_3O_4. The mean crystal diameter of the Fe_3O_4 (D) could be calculated from the (311) plane refraction peak with the Scherer equation:

$$D=K\lambda/(b\cos\theta) \quad (2)$$

where λ is the X-ray wavelength (1.5418 Å), b is the width of the peak at half height at angle θ, and K is a shape factor of about 0.9 for magnetite.[21] The mean crystal diameter of the Fe_3O_4 nanoparticles was thus calculated to be 7.6 nm. At the same time, it was interesting to note the disappearance of the diffraction peak of CS in the XRD pattern of the composite material. We thought that this resulted from the presence of the Fe_3O_4 nanoparticles, which might have interacted with the CS molecules to interfere with the crystallization of CS.

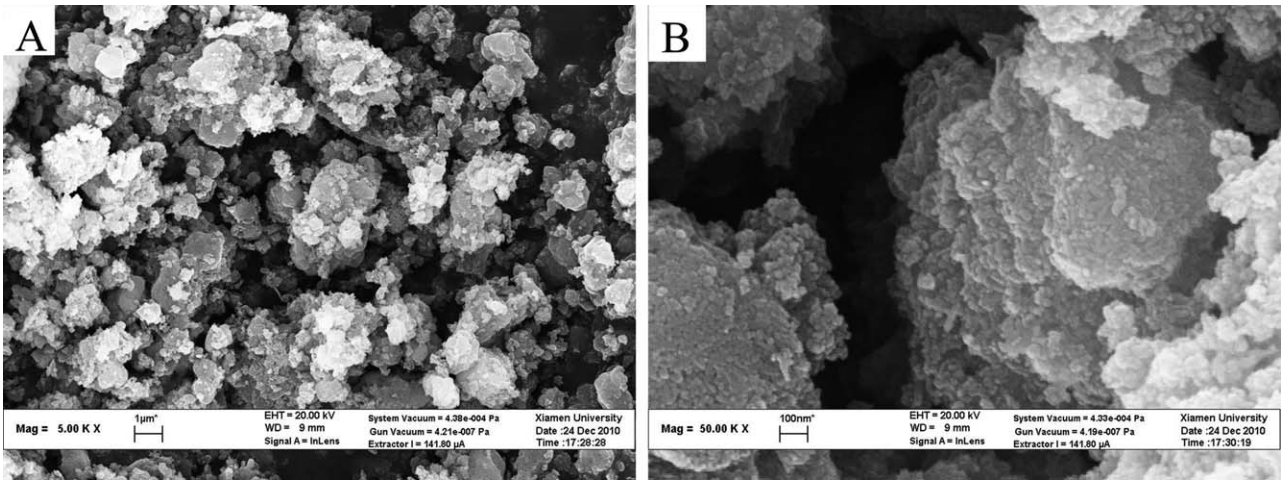

Figure 1. SEM images of the composite material under different magnifications.

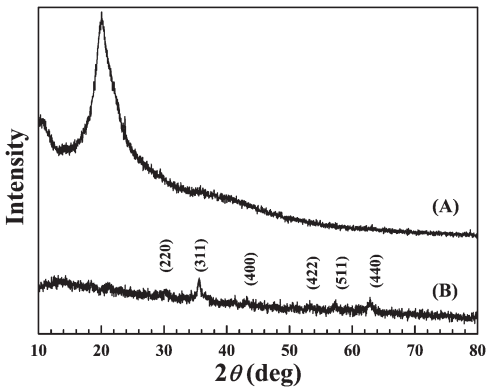

Figure 2. XRD patterns of the (A) pure CS and (B) magnetic CS composite material.

The TEM images of the composite material are shown in Figure 3. We observed in Figure 3(A) that the black dots of the formed Fe_3O_4 nanoparticles were evenly dispersed, and no obvious agglomerate of the nanoparticles was found. The size of the Fe_3O_4 nanoparticles was evaluated from the TEM image to be in the range 3–7 nm, and this was consistent with the XRD results. The high-resolution TEM image of the Fe_3O_4 shown in Figure 3(B) indicated that each particle was a well-ordered single crystal. The distance between the two adjacent lattice fringes was measured to be about 0.25 nm, which corresponded to a lattice spacing of the (311) plane of cubic magnetite.[22] This finding led to a new preparation of an Fe_3O_4 single nanocrystal with a diameter ranging from 3 to 7 nm, which had the potential to be applied as a contrast agent and will be discussed in another article. The TEM results suggested that the Fe_3O_4 nanoparticles were firmly stabilized by the CS matrix; this indicated interaction between the Fe_3O_4 nanoparticles and CS chains. We noted that the formed Fe_3O_4 particles were smaller than those coprecipitated from the Fe^{3+}/Fe^{2+}/CS mixture solution by the addition of an ammonia aqueous solution.[17,23] The Fe_3O_4 particles formed in the latter case were stabilized by the coexisting CS molecules and were at the scale of several 10s of nanometers. The results suggest that the formation of the Fe_3O_4 nanoparticles might have been different under these conditions.

Figure 4 shows the FTIR spectra of the pure CS and the composite material. For pure CS, the peaks around 899 and 1156 cm^{-1} were assigned to its saccharide structure. The characteristic bands of amide I, amide II, and amide III for CS were

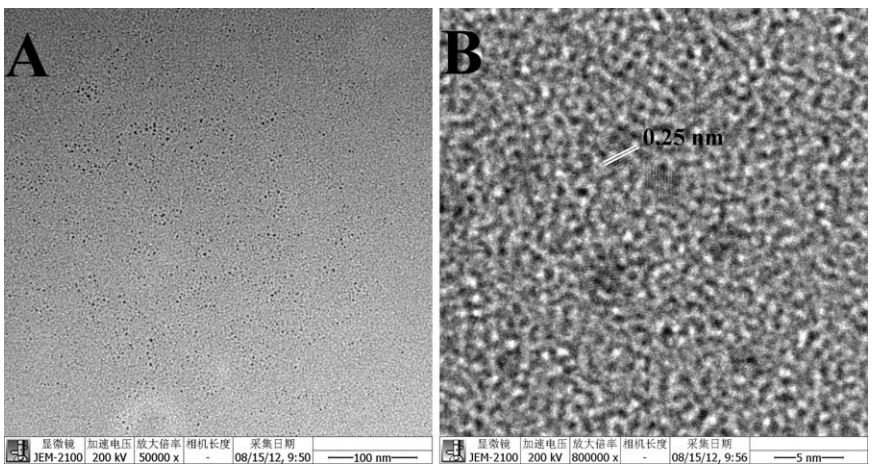

Figure 3. (A) TEM and (B) high-resolution TEM images of the magnetic CS composite material.

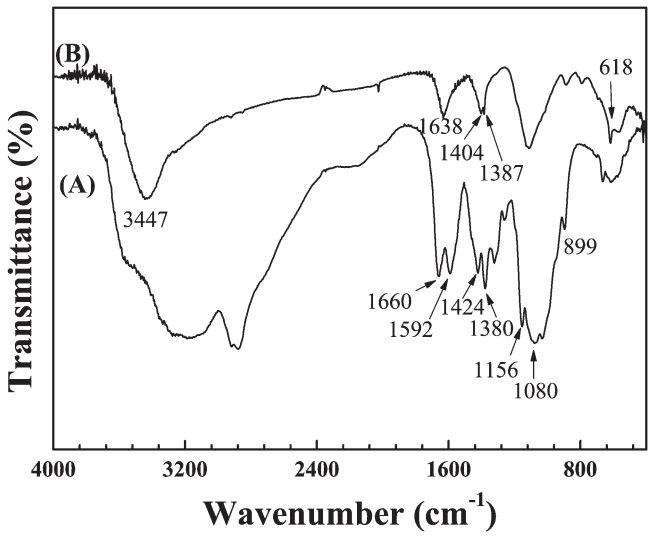

Figure 4. FTIR spectra of the (A) pure CS and (B) composite material.

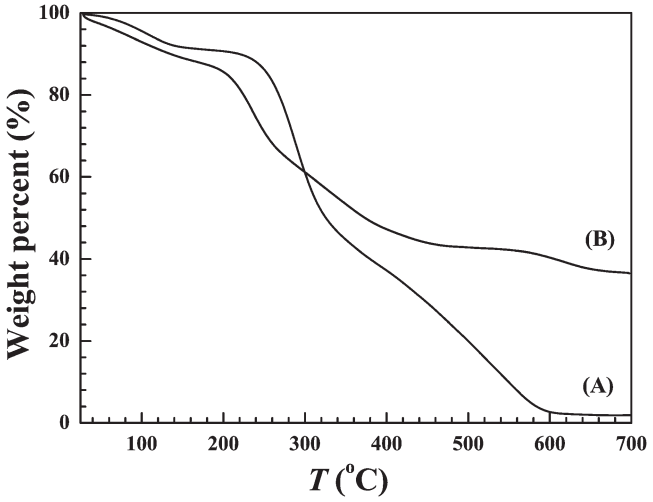

Figure 5. TGA curves of the (A) pure CS and (B) composite material (T = temperature).

found at 1660, 1592, and 1380 cm^{-1}, respectively. The peak at 1424 cm^{-1} was attributed to the —NH deformation vibration of the amine groups belonging to CS. The spectrum of the final composite material was similar as that of pure CS except that some peaks shifted to lower or to higher frequencies. When the XRD results were combined, the relatively strong band at 618 cm^{-1} in the spectrum was assigned to magnetite (Fe_3O_4).[24] Therefore, the obvious shifts of the aforementioned characteristic bands of CS were attributed to the presence of the Fe_3O_4 nanoparticles in the CS matrix. At the same time, the shifts indicated strong interaction due to complexation between the amine groups and the carbonyl oxygen of CS and the Fe_3O_4 nanoparticles.[16,17,24–27] As a result, the interaction benefited the stabilization of the formed Fe_3O_4 nanoparticles by the neighboring CS molecules and prevented them from agglomerating; this was consistent with the SEM and TEM observations. The interaction between the CS and Fe_3O_4 nanoparticles may also interfere with the crystallization of CS, as illustrated in Figure 2.

It is known that a polymer such as CS can be used as a flocculating agent because of its abundant functional groups, including amino and hydroxyl groups, can bind cations such as heavy-metal ions. Those functional groups will be protonized when CS is dissolved in an acidic acid solution. When it is mixed with an aqueous solution of $NH_4Fe(SO_4)_2$/$(NH_4)_2Fe(SO_4)_2$, the protonized functional groups along the CS chains will bind the oppositely charged $[Fe(SO4)_2]^-$ and $[Fe(SO4)_2]^{2-}$ ions because of the electrostatic interaction and coordination.[24,28] As a result, the CS chains will precipitate so one can obtain the intermediate flocculation product, which might be in the swollen state. After an ammonia fumigation treatment, the swollen CS will precipitate further, whereas the Fe ions might be transferred into ferrous hydroxide and ferric hydroxide. Upon dehydration, the ferrous hydroxide and the ferric hydroxide will transform into Fe_3O_4 because of its lowest Gibbs energy (−242.7 kJ/mol, 298.15 K) when compared with FeO (−60.1 kJ/mol, 298.15 K) and Fe_2O_3 (−177.4 kJ/mol, 298.15 K).[29]

It is easy to conceive that the $[Fe(SO4)_2]^-$ and $[Fe(SO4)_2]^{2-}$ ions would be homogeneously distributed in the intermediate flocculation product because of their binding with the functional groups along the CS chains as the consequently formed ferrous hydroxide and ferric hydroxide do after an ammonia fumigation treatment. However, the following formation of Fe_3O_4 by dehydration would drive the ferrous hydroxide and the ferric hydroxide to enrich at somewhere in the CS matrix. It is worth noting that the Fe_3O4 transformation was carried out by an ammonia fumigation treatment, which limited the immigration of the aforementioned ferrous hydroxide and ferric hydroxide. Therefore, the formation of Fe_3O_4 could only take place locally to obtain the 3–7-nm Fe_3O_4 nanoparticles, which were then stabilized by the CS matrix because of their interaction. However, the immigration of the ferrous hydroxide and ferric hydroxide in the coprecipitation method made it much easier for bigger Fe_3O_4 nanoparticles to be formed because the enrichment of the components took place in homogeneous media.[17,30]

Properties

The Fe_3O_4 content in the composite adsorbent was determined by TGA. Figure 5 shows the thermograms of the pure CS and the composite material. The pure CS exhibited three obvious stages of weight losses, which corresponded to the removal of absorbed water, the thermal decomposition of CS, and the oxidation of charred CS.[17] The ash content of CS was thus determined to be 1.9%. The composite material displayed a similar thermal behavior. However, an almost constant weight residue was found for the composite when the temperature was higher than 650°C; this suggested the presence of only iron oxide and ash. Therefore, the weight content of Fe_3O_4 in the composite was calculated to be 39.1%.

The magnetic properties of the composite material were measured with VSM, and the results are shown in Figure 6. The invisible hysteresis [Figure 6(A)] suggested the superparamagnetic properties of the material. The saturation magnetization

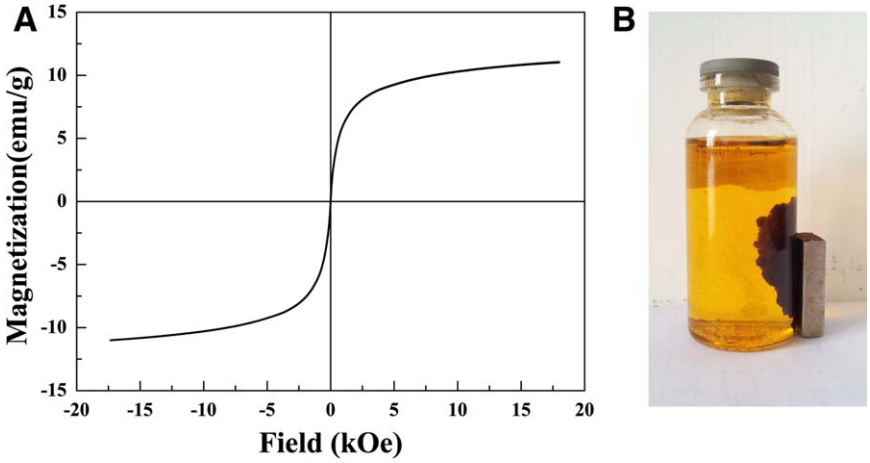

Figure 6. (A) Hysteresis loop of the magnetic CS composite material at 27°C and (B) a photograph showing the response of the composite material to an external magnetic field in the MO solution. [Color figure can be viewed in the online issue, which is available at wileyonlinelibrary.com.]

of the composite material determined from the hysteresis loop was 11.0 emu/g; this suggested that the composite material was suitable for fast response to an external magnetic field [Figure 6(B)] and facile removal from the liquid phase after adsorption. The composite could be easily dispersed by shaking once the applied magnetic force was removed.

Adsorption

The adsorptions of Cu^{2+} and MO were carried out at pH around 5.5 with a 10 μg/mL initial concentration of the adsorbate. Figure 7 shows the results, which exhibit a similar adsorption behavior of Cu^{2+} and MO on the composite material. We observed that the adsorptions took place quickly, and the adsorption amounts of both adsorbates seemed to reach maxima at about 200 min. The adsorption kinetics were also modeled by the Langmuir isotherm, which reads as follows:[31]

$$Q = Q_{max}\frac{kt}{1+kt} \quad (3)$$

where k is a constant related to the adsorption speed and t is the adsorption time. We found that the data points could be well modeled, and the parameters are collected in Table I. The evaluation of the data points yielded Q_{max} values of 5.64 and 4.70 mg/g and k values of 0.0264 and 0.0303 min^{-1} for Cu^{2+} and MO, respectively. The adsorption capacities were comparable with those of CS-based magnetic adsorbents reported in the literature.[13,14,31,32] Meanwhile, the correlation coefficients (R^2's) were 0.9973 and 0.9906 for Cu^{2+} and MO adsorption, respectively; this indicated Langmuir monolayer adsorption.[31] The adsorption mechanism of the composite was thought to be based on the cationic nature of CS, where the protonated amino groups could bind metal ions or dye molecules through various types of interactions, such as electrostatic attractions and chelation.[13,31,32]

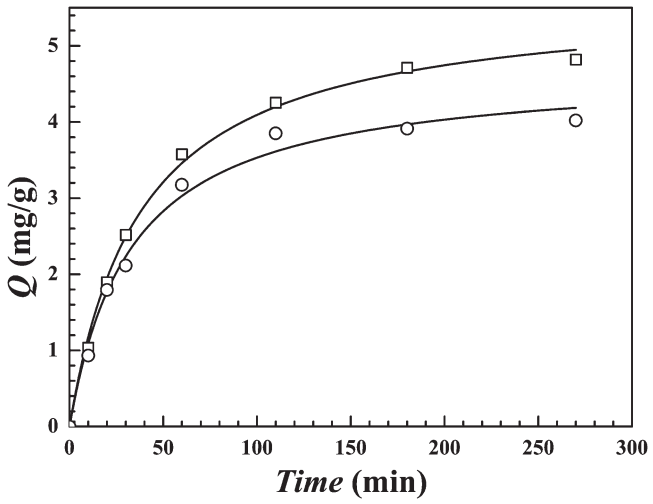

Figure 7. Adsorption of Cu^{2+} and MO on the magnetic CS composite adsorbent.

Table I. Parameters of the Adsorption of Cu^{2+} and MO on the Magnetic CS Composite Adsorbent According to Langmuir Isotherm Modeling

Adsorbate	Q_{max} (mg/g)	k (min^{-1})	R^2
Cu^{2+}	5.64	0.0264	0.9973
MO	4.70	0.0303	0.9906

CONCLUSIONS

A magnetic CS composite material was successfully synthesized by a new method of ammonia fumigation treatment. The heterogeneous reaction of the magnetite precursors limited their immigrations, leading to *in situ* formation of 3–7-nm Fe_3O_4 nanoparticles; these were much smaller than the Fe_3O_4 nanoparticles prepared by the usual coprecipitation method in a homogeneous medium.[17] The composite material showed superparamagnetic properties and displayed a quick response to an external magnetic field. At the same time, the composite revealed good adsorptions of MO and copper ions. This new method for the preparation of magnetic CS composite materials is thought to be practical in view of the easy fabrication process.

ACKNOWLEDGMENTS

This work was funded by the Natural Science Foundation of China (contract grant number 51273166), the Natural Science Foundation of Fujian Province of China (contract grant number 2013J01206), and the National Basic Research Program of China (973 Program, contract grant number 2010CB732203).

REFERENCES

1. Zhang, J. M.; Zhang, J. *Acta Polym. Sinica* **2010**, *12*, 1376.
2. Kumar, P.; Guliants, V. V. *Micropor. Mesopor. Mater.* **2010**, *132*, 1.
3. Haberkorn, N.; Lechmann, M. C.; Sohn, B. H.; Char, K.; Gutmann, J. S.; Theatol, P. *Macromol. Rapid. Commun.* **2009**, *30*, 1146.
4. Lin, X. Z.; Ma, T. Y.; Yuan, Z. Y. *Chem. Eng. J.* **2011**, *166*, 1144.
5. Thanganathan, U. *J. Mater. Chem.* **2011**, *21*, 456.
6. Julián-López, B.; Boissière, C.; Chanéac, C.; Grosso, D.; Vasseur. S.; Miraux, S.; Duguet, E.; Sanchez, C. *J. Mater. Chem.* **2007**, *17*, 1563.
7. Vemula, P. K.; Douglas, K.; Achong, C.; Kumar, A.; Ajayan, P.; John, G. *J. Biobased Mater. Bioenergy* **2008**, *2*, 218.
8. Li, L. L.; Fang, C. J.; Sun, H.; Yan, C. H. *Chem. Mater.* **2008**, *20*, 5977.
9. Sotiropoulou, M.; Bokias, G.; Staikos, G. *Biomacromolecules* **2005**, *6*, 1835.
10. Dubin, P. L.; Gao, J.; Mattison, K. *Sep. Purif. Rev.* **1994**, *23*, 1.
11. Halder, A.; Maiti, S.; Sa, B. *Int. J. Pharm.* **2005**, *302*, 84.
12. Shi, X.; Du, Y.; Sun, L.; Zhang, B.; Dou, A. *J. Appl. Polym. Sci.* **2006**, *100*, 4614.
13. Arruebo, M.; Fernández-Pacheco, R.; Ibarra, M. R.; Santamaría, J. *Nano Today* **2007**, *2*, 22.
14. Chang, Y. C.; Chen, D. H. *J. Colloid Interface Sci.* **2005**, *283*, 446.
15. Wang, Y.; Wang, X.; Luo, G.; Dai, Y. *Bioresour. Technol.* **2008**, *99*, 3881.
16. Denkbaş, E. B.; Kiliçay, E.; Birlikseven, C.; Öztürk, E. *React. Funct. Polym.* **2002**, *50*, 225.
17. Zou, W.; Geng, H.; Lin, M.; Xiong, X. *J. Appl. Polym. Sci.* **2012**, *123*, 3587.
18. Xiong, X.; Duan, J.; Zou, W.; He, X.; Zheng, W. *J. Membr. Sci.* **2010**, *363*, 96.
19. Zhou, Y.; Wang, F.; Kim, Y.; Kim, S. J.; Yoon, J. *Org. Lett.* **2009**, *11*, 4442.
20. Li, Y.; Li, X.; Li, J.; Yin, J. *Water Res.* **2006**, *40*, 1119.
21. Qu, J.; Liu, G.; Wang, Y.; Hong, R. *Adv. Powder Technol.* **2010**, *21*, 461.
22. Schertmann, U.; Cornell, R. M. Iron Oxides in the Laboratory: Preparation and Characterization, 2nd ed.; Wiley: New York, **2000**.
23. Ge, J. P.; Hu, Y. X.; Biasini, M.; Dong, C. L.; Guo, J. H.; Beyermann, W. P.; Yin, Y. D. *Chem.—Eur. J.* **2007**, *13*, 7153.
24. Massart, R. *IEEE Trans. Magn.* **1981**, *17*, 1247.
25. Arami, M.; Limaee, N. Y.; Mahmoodi, N. M.; Tabrizi, N. S. *J. Hazard. Mater.* **2006**, *135*, 171.
26. Chernichko, D. I.; Khomutov, G. B. *Inorg. Mater.* **2009**, *45*, 1370.
27. Laus, R.; Costa, T. G.; Szpoganicz, B.; Fávere, V. T. *J. Hazard. Mater.* **2010**, *183*, 233.
28. Wang, J.; Peng, R.; Yang, J.; Liu, Y.; Hu, X. *Carbohydr. Polym.* **2011**, *84*, 1169.
29. Dean, J. A. In Lange's Handbook of Chemistry, 1988, 15th ed.; Science Press: Beijing, **2003**, p 981 (Chinese translation version, by Wei, J. F.).
30. Wu, K. T.; Kuo, P. C.; Yao, Y. D.; Tsai, E. H. *IEEE Trans. Magn.* **2001**, *37*, 2651.
31. Singh, A. K.; Quraishi, M. A. *Corros. Sci.* **2010**, *52*, 152.
32. Wan Ngah, W. S.; Teong, L. C.; Hanafiah, M. A. K. M. *Carbohydr. Polym.* **2011**, *4*, 1446.